

Full-Potential LAPW calculation of electron momentum density and related properties of Li

Tunna Baruah, Rajendra R. Zope and Anjali Kshirsagar *

Department of Physics, University of Pune, Pune-411007, India

(July 5, 2021)

Electron momentum density and Compton profiles in Lithium along $\langle 100 \rangle$, $\langle 110 \rangle$, and $\langle 111 \rangle$ directions are calculated using Full-Potential Linear Augmented Plane Wave basis within generalized gradient approximation. The profiles have been corrected for correlations with Lam-Platzman formulation using self-consistent charge density. The first and second derivatives of Compton profiles are studied to investigate the Fermi surface breaks. Decent agreement is observed between recent experimental and our calculated values. Our values for the derivatives are found to be in better agreement with experiments than earlier theoretical results. Two-photon momentum density and one- and two-dimensional angular correlation of positron annihilation radiation are also calculated within the same formalism and including the electron-positron enhancement factor.

I. INTRODUCTION

Compton scattering and positron annihilation techniques are well established tools for studying the momentum distribution of electrons in solids¹⁻⁴. In the Compton scattering technique, the intensity distribution of energy broadened Compton scattered radiation (called the Compton profile) is studied while in positron annihilation technique, measurement of angular correlation between two photons emitted during the annihilation of a thermalized positron with electrons in the solid, is performed. The Compton profile (CP) and angular correlation of positron annihilation radiation (ACPAR) curves contain the finger prints of the Fermi surface (FS) breaks in the momentum distribution in the first and higher Brillouin zones. It is well known that although the magnitude of the discontinuity in momentum distribution itself changes due to electron-electron, electron-ion and electron-positron correlations, the position of the discontinuity remains unchanged⁵⁻⁷. Thus, these techniques together are useful to extract information about FS geometry and to identify electron correlation effects. Positron annihilation techniques are more sensitive to the outer, weakly bound conduction electrons and are also capable of performing measurements in both one-dimensional and two-dimensional geometries, with much superior momentum resolution. Theoretically, however, it is more straight for-

*Author to whom all correspondence should be directed.

ward to calculate CP's as ACPAR studies necessitate to account for electron-positron many-body correlation effects. These effects are incorporated in the form of momentum, energy or density dependent enhancement factors⁸⁻¹².

Early measurements of Compton profile were suffering from the limited momentum resolution in the Compton scattering experiment ($\sim 0.4a.u.$). The advent of high intensity, high energy and well-polarized synchrotron sources and the spectrometers with high resolution ($\sim 0.12a.u.$) have resulted in revival of interest in this area¹³⁻¹⁵. On the theoretical side, high performance computing facilities have made it possible to perform calculations on a fine \vec{p} -mesh with a better convergence criteria for the total energy and charge density self-consistency.

In the present communication, we report full potential linearized augmented plane wave (FP-LAPW) calculations of the electron momentum distribution in *Li*. In lithium, because of its smallness, the electron-ion interactions are strong and the electrons do not behave like a text-book example of homogeneous electron gas as in sodium. The Fermi surface of *Li* shows a small but definite departure from free electron sphere. The electron momentum density is highly anisotropic, the high momentum components (HMCs) are small but important. The momentum distribution of *Li* has been investigated in the past, both theoretically and experimentally, by several workers¹⁶⁻²⁰ with the available state-of-the-art procedures. Recently, Sakurai *et al.*¹³ have performed high resolution Compton scattering experiments for *Li* to measure Compton profiles and Fermi radii. The measured CP's are compared with the theoretical ones calculated using KKR method. Subsequently, Schülke and coworkers¹⁵ measured 11-directional Compton profiles and employed them to reconstruct the three dimensional EMD in *Li* metal. The comparison of the experimental CP's with their theoretical counterparts have always shown some discrepancies. This is partly due to the various approximations involved in computing the profile and partly due to the experimental errors. The methods like FP-LAPW can provide accurate results for the one-electron wavefunction and hence should be employed for computation of theoretical CP's. Such accurate calculations of the CP's of *Li* have been reported by Kubo^{21,22} employing the GW approximation using FP-LAPW wavefunctions within local density approximation (LDA) as the zeroth approximation. The calculated CP's are in good agreement with the experimental values but the derivatives of the CP's match the experimental ones poorly²¹. The derivatives of CP's are important as they provide information about the Fermi surface.

In the present paper, we use full-potential linearized augmented plane wave method for the computation of CP which have been corrected to include the correlation effects not accounted for within LDA, alongwith one and two dimensional angular correlation of positron annihilation radiation (1D- and 2D-ACPAR) which include corrections due to electron-positron correlation effects. Such studies using the same formalism for calculation of CP and ACPAR can provide complementary information about the Fermi surface and the electron momentum distribution. Our aim in this communication is to extract the FS geometry from the two techniques together and to identify the part of

electron correlations left out in the theory to describe the EMD. The plan of the paper is as follows: in section II, we present the momentum space formulation of the LAPW wavefunction and computational details, while section III deals with the results.

II. METHODOLOGY AND COMPUTATIONAL DETAILS

The one electron wavefunction for an electron in the state labeled by wave vector \vec{k} and band index j is expanded in the Linearized Augmented Plane Wave (LAPW) basis $\phi_{\vec{k}+\vec{G}}(\vec{r})$ as

$$\psi_{\vec{k}}^j(\vec{r}) = \sum_{\vec{G}} c_{\vec{k}+\vec{G}}^j \phi_{\vec{k}+\vec{G}}(\vec{r}), \quad (1)$$

where $c_{\vec{k}+\vec{G}}^j$ are the expansion coefficients and \vec{G} denotes reciprocal lattice vector. The LAPW function is a plane wave outside the MT sphere while inside it is a linear combination of $u_l(r)$, the solution of the radial Schrödinger equation and its energy derivative $\dot{u}_l(r)$. This allows greater flexibility inside the spheres (than the APW method) and hence permits computation of an accurate solution²³.

The momentum space LAPW wavefunction is obtained by a Dirac-Fourier transformation of eq. (1) and the electron momentum density is computed from the momentum space wavefunction of occupied states. The Compton profile is then obtained by performing a double integral.

The theoretical Compton profile thus obtained is overestimated at low momenta and is underestimated at higher momentum values than its experimental counterpart. This discrepancy is often attributed to the correlation effects that are ignored in the independent particle model²⁴. Lam and Platzman²⁴ have shown that these effects can be incorporated into the EMD by augmenting to the independent electron model momentum density a correction term. The recent formulation of Cardwell and Cooper²⁵ based on the Lam-Platzman work which takes care of the non-unity occupation below the Fermi momentum k_f and non-zero occupation beyond k_f has been employed in the present work.

For a single positron in a defect free crystal, the positron density will be distributed over the entire crystal. Therefore, the positron wavefunction, $\psi_+(\vec{r})$, is considered to be delocalized and is represented by a plane wave basis. Further, as the positron essentially thermalizes before annihilation, it is assumed to be in the state $\vec{k}_+ = 0$. The enhancement in the TPMD due to the electron-positron short-range correlation is calculated according to the prescription given by Puska *et al.*¹⁰ which is a function of electron and positron densities. Thus, TPMD is evaluated using the following prescription :

$$\rho^{2\gamma}(\vec{p}) = \sum_{\vec{k}, j}^{occ} |F_{\vec{k}}^j(\vec{p})|^2 = \sum_{\vec{k}, j}^{occ} \left| \int e^{-i\vec{p}\cdot\vec{r}} \psi_+(\vec{r}) \psi_{\vec{k}}^j(\vec{r}) \sqrt{g(n^e(\vec{r}), n^+(\vec{r}))} d^3r \right|^2. \quad (2)$$

where $n^e(\vec{r})$ and $n^+(\vec{r})$ are the electron and positron densities respectively and the enhancement factor $g(n^e(\vec{r}), n^+(\vec{r}))$ in the limit $n^+(\vec{r}) \rightarrow 0$ is

$$g_0(r_s) = 1 + 1.23r_s + 0.98890r_s^{3/2} - 1.4820r_s^2 + 0.3956r_s^{5/2} + r_s^3/6 \quad (3)$$

where $r_s = \left[\frac{3}{4\pi n^e(\vec{r})} \right]^{1/3}$.

A self-consistent band-structure calculation was performed using the LAPW method as implemented in WIEN97 package²⁶. The calculation employs full potential which implies that the nonspherical part of the potential inside the muffin-tin sphere and its deviation from the constant potential in the interstitial region are taken into consideration. The simplified generalized gradient approximation (GGA) due to Perdew *et al.*²⁷ was used for the exchange-correlation part of the Kohn-Sham potential. In the band structure calculation the lattice constant of *Li* in bcc structure is taken to be $6.61375a.u.$ ²⁸. The self-consistency cycles were carried out to an energy tolerance of 10^{-6} Ryd and charge convergence of 10^{-5} electrons. The various band-structure parameters agree very well with earlier accurate calculations^{20,29}.

For the calculation of Compton profile, in 1/48th of the Brillouin zone (BZ) we used 40425 \vec{k} -points to evaluate the momentum space wavefunction which when translated by the reciprocal space vectors yield 40425×531 \vec{p} -points. Linear tetrahedron method³⁰ was used for the calculation of Compton profiles over a momentum mesh of $0.001a.u.$. The correlation correction was carried out as described by Cardwell *et al.*²⁵. In carrying out these calculations we used the self-consistent density inside the MT sphere whereas in the interstitial region we assumed the density to be flat with little structure. No r_s cut-off value was used as suggested by Cardwell *et al.*²⁵.

For the calculation of two photon momentum density, the wavefunction for the positron was obtained by solving the secular determinant once using the self-consistent Coulombic potential from earlier calculation for electronic band structure but with an opposite sign. We have used 819 \vec{k} -points to evaluate $F_k^j(\vec{p})$.

III. RESULTS AND DISCUSSION

The electron momentum density for lithium metal along $\langle 100 \rangle$, $\langle 110 \rangle$ and $\langle 111 \rangle$ directions in the momentum space is plotted in Fig. 1. Each panel shows EMD along one direction, calculated within LDA and GGA employing von Barth-Hedin (VBH)³¹ and Perdew-Burke-Ernzerhof (PBE)²⁷ exchange-correlation potentials respectively alongwith GGA-EMD corrected using Lam-Platzman (LP)²⁴ correction term in that direction employing the model momentum density proposed by Cardwell *et al.*²⁵. The results are almost identical for VBH and PBE exchange-correlation potentials indicating that the non-local corrections as described within GGA do not seem to

affect the momentum density in Li although the electronic structure is slightly different in LDA and GGA. This gives rise to almost identical Compton profiles (CPs) for LDA and GGA formulations as predicted by Lam and Platzman³². These observations for Li support the fact that although the ionic potential is strong in Li , the conduction electron density behaves more like a homogeneous electron gas. Similar calculations for transition metals do show significant differences in LDA and GGA results³³.

The strong ionic periodic potential, however, does couple the states near Brillouin zone (BZ) boundaries and the conduction electron wavefunctions contain strong high momentum components and the EMD does show anisotropic behavior as is evident from Fig. 1. Since Li has only one electron in the conduction band, in the one-electron picture, the EMD is zero beyond k_f in the first BZ and between its images in higher zones. Lam-Platzman²⁴ correction partly takes care of the correlation effects on the wavefunctions in one-electron picture. The occupation number of an interacting homogeneous electron gas is estimated to be smaller than that of a non-interacting free electron gas by 4% for Li ⁷. Our LP corrected EMD displays the effect of states below k_f being pushed above k_f in Li and these can be compared with results in Fig. 5 of ref.¹⁷ which uses mean occupation numbers derived from electron gas data for correlation effects and couples them with orthogonalized plane wave band structure method. EMD dies off in higher zones along $\langle 100 \rangle$ and $\langle 111 \rangle$ directions but shows a strong umklapp component along $\langle 110 \rangle$ direction. These higher momentum components (HMCs) play an important role in determining the shapes of Compton profiles and angular correlation curves.

Compton profiles $J_{\hat{k}}(q)$ corrected for the correlations are presented in Fig. 2 together with the experimental and KKR results¹³ with \hat{k} along $\langle 100 \rangle$, $\langle 110 \rangle$ and $\langle 111 \rangle$ directions. In order to facilitate the comparison with experimental CP's, the theoretical CP's were convoluted with a Gaussian of FWHM of 0.12 a.u. (experimental resolution in ref.¹³). Our Compton profiles, when compared with experimental values, support the widely known behavior, namely, overestimation at low momentum and underestimation at higher momentum values. Correlation corrections lower the CP values within the main Fermi surface but they are still higher than the experimental results. It is to be noted that KKR values are consistently higher than our values near $q = 0$ and show a more pronounced cusp like behavior near \vec{k}_f for all the three directions. The cusp seen in CP reflects the discontinuity in EMD at \vec{k}_f in the first BZ and their images in higher zones. The results indicate that the discontinuity is smaller in FP-LAPW calculations than in KKR. The disagreement between present results and KKR results could be attributed to the fact that present work is a full potential calculation whereas KKR uses muffin-tin shape approximation. Secondly, the LP correction has been calculated using the prescription of Cardwell *et al.*²⁵ employing self-consistent charge density in the present work whereas KKR uses interpolated results from homogeneous electron gas data. Our results agree with those of KKR beyond $q = 0.8$ a.u. while the experimental values are consistently higher than the theory in this region.

This reflects that the non-zero occupation beyond \vec{k}_f for the inhomogeneous electron gas is only partially accounted for by the theory.

We have also compared the directional anisotropies in the Compton profiles with the experimental work of Sakurai *et al.*¹³ and the overall agreement is found to be good. The directional anisotropies are important while comparing theory with experiment as the systematic errors in the experimental and theoretical results are canceled out. The prominent structures near $q = 0$ are well reproduced at the correct momentum values, however, they are overestimated by theory (Fig. 3). This is again due to the correlation correction functional as discussed by Bauer *et al.*³⁴. In the present calculation, we have included the correlation correction which is isotropic and therefore does not affect the results of anisotropy. Attempts to include anisotropic corrections are in progress and will be published elsewhere.

The two-dimensional ACPAR surfaces were obtained by integrating $\rho^{2\gamma}(\vec{p})$ along $\langle 100 \rangle$, $\langle 110 \rangle$ and $\langle 111 \rangle$ directions respectively; while the one dimensional curves were obtained using the linear tetrahedron method. The 1D ACPAR curves along $\langle 100 \rangle$, $\langle 110 \rangle$ and $\langle 111 \rangle$ are shown in Fig. 4 and are in qualitative agreement with earlier published work^{35,36}. The 1D ACPAR curves were convoluted with a Gaussian with FWHM of 0.022 a.u.. The 2D ACPAR data convoluted with 0.5×0.23 mrad² FWHM³⁷ is presented in Fig. 5 and the overall shape matches with experiment³⁸. The higher momentum components in TPMD are seen quite clearly in the 2D ACPAR plot. The smaller bump comes from the TPMD in the second zone in the $\langle 110 \rangle$ direction, whereas the contributions from higher zones are hardly visible. The larger bump is a result of projected contributions from $\langle 01\bar{1} \rangle$ and $\langle 10\bar{1} \rangle$ for the same p value. The HMC intensity is seen to be a sharp function of momentum values. The momentum density decreases with increasing momentum values which is a direct reflection of s -like wavefunction.

We have extracted relevant FS data from both electron and electron-positron momentum distributions. Although, in principle, both the Compton scattering and the ACPAR probe the electron momentum distribution and provide complementary information about FS, the latter however provides the best possible measurements for FS breaks in EMD since the electron-positron correlations enhance the momentum density at k_f . The prominent breaks in momentum distribution are seen around 0.6 a.u. with slightly different values along different directions as shown in Fig. 1 for EMD. Similar structure is seen in TPMD also. The images of the FS breaks, seen in higher zones due to periodicity, are reflected in the CP and ACPAR data. The structures seen are identical to those seen earlier and discussed by Sakurai *et al.*¹³ for CP and Stewart *et al.*³⁵ for ACPAR curves. However, we point out that the LP correction shifts the FS breaks as seen in the derivatives of CP. This is a limitation of the model which employs isotropic momentum density to calculate the LP correction.

Figure 6 displays the first derivatives of the directional Compton profiles. Although the breaks in the first derivative curve without convolution bring out the structures rather well indicating the distortions of the free electron sphere,

however, in Fig. 6, we show the derivatives of the convoluted Compton profiles to facilitate comparison with experimental results. The derivatives of 1D ACPAR which bring out the FS breaks sharply are presented in Fig. 7. The values of the FS radii along the principal symmetry directions $\langle 100 \rangle$, $\langle 110 \rangle$ and $\langle 111 \rangle$ as estimated from the positions of peaks in the second derivatives of CP differ from the actual Fermi radii as described by Sakurai *et al.*¹³. The first derivatives of directional ACPAR curves give the correct Fermi radii since the high momentum components in TPMD are smaller. Our values of Fermi radii alongwith the experimental values¹³ are presented in Table I. The maximum Fermi surface asphericity, $[k_{110} - k_{100}]/k_f^0$ where k_f^0 is the free electron radius, in our calculation turns out to be 5.6% against the experimental value of 4.6%, 5% and 4.7% respectively obtained from CP¹³, 1D-ACPAR³⁹ and 2D-ACPAR data³⁷.

In this paper, we have presented the Compton profiles computed using FP-LAPW method within GGA and have corrected them for correlations on the lines of Cardwell and Cooper²⁵ using self-consistent charge density. The derivatives of the calculated CP's are in good agreement with their experimental counterparts. Usually, the discrepancy between theory and experiment is ascribed to the limitation of local density approximation. However, we have seen that gradient corrections to exchange-correlation potential as described in GGA do not affect the electron momentum density significantly. In principle, Lam-Platzman correction describes the non-local effects on the momentum density correctly but the practical implementation is able to account for it only partly, namely the isotropic electron correlations are described satisfactorily but not the anisotropic ones. Although Bauer *et al.*³⁴ have rejected the idea of momentum density functional theory, we feel a description for the exchange-correlation energy functional in momentum space will allow a better quantitative representation of EMD theoretically.

One and two dimensional ACPAR curves are also computed using the FP-LAPW method. We have shown that the different shapes of HMCs are well reproduced by our calculations. Inclusion of density dependent enhancement factor is found to reduce the HMCs at large p values. To our knowledge, this is the first theoretical report of 1D- and 2D-ACPAR for *Li* incorporating density dependent enhancement effects.

ACKNOWLEDGMENTS

We gratefully acknowledge the experimental data and KKR results provided by Dr. Y. Sakurai and Prof. A. Bansil. We are grateful to Prof. K. Schwarz and Dr. P. Blaha for providing the WIEN97 code. We are also thankful to Dr. V. Sundarajan and Prof. R. M. Singru for helpful discussions. TB and RRZ gratefully acknowledge the financial support from Council for Scientific and Industrial Research, New Delhi in the form of fellowships.

-
- ¹ B. G. Williams (ed.), *Compton Scattering*, (McGraw Hill, GB, 1977).
- ² R. M. Singru, in *Positron Annihilation*, edited by P. G. Coleman, S. C. Sharma and L. M. Diana, (North-Holland, Amsterdam, 1982);
- ³ R. N. West, in *Positron Annihilation*, edited by P. C. Jain, R. M. Singru and K. P. Gopinathan, (World Scientific, Singapore, 1985).
- ⁴ S. Berko and J. S. Laskett, Phys. Rev. **112**, 1877 (1958); A. T. Stewart and L. O. Roelling, (eds.), *Positron Annihilation*, (Academic Press, New York, 1967); A. P. Mills Jr., W. S. Crane and K. F. Canter, (eds.), *Positron studies of solids, surfaces and atoms*, (World Scientific, Singapore, 1986).
- ⁵ C. K. Majumdar, Phys. Rev. **140**, A 227 (1965).
- ⁶ A. B. Migdale, Zh. Eksp. Teor. Fiz. **5**, 399 (1957) [Sov. Phys. JETP. **5**, 333 (1957)].
- ⁷ E. Daniel and S. H. Vosko, Phys. Rev. **120**, 2041 (1960).
- ⁸ S. Kahana, Phys. Rev. **129**, 1622 (1963).
- ⁹ P. E. Mijnarends and R. M. Singru, Phys. Rev. B. **19**, 6038 (1979).
- ¹⁰ M. J. Puska, A. P. Seitsonen and R. M. Nieminen, Phys. Rev. B **52**, 10947 (1995).
- ¹¹ T. Jarlborg and A. K. Singh, Phys. Rev. B **36**, 4660 (1987).
- ¹² S. Daniuk, G. Kontrym-Sznajd, A. Rubaszek, H. Stachowiak, J. Mayers, P. A. Walters and R. N. West, J. Phys. F **17**, 1365 (1987).
- ¹³ Y. Sakurai, Y. Tanaka, A. Bansil, S. Kaprzyk, A. T. Stewart, Y. Nagashima, T. Hyodo, S. Nanao, H. Kawata and N. Shiotan, Phys. Rev. Lett. **74**, 2252 (1995).
- ¹⁴ M. A. G. Dixon, J. A. Duffy, S. Gardelis, J. E. McCarthy, M. J. Cooper, S. B. Dugdale, T. Jarlborg and D. N. Timms, J. Phys. Cond. Matt. **10**, 2759(1998); M. J. Cooper, Radiat. Phys. Chem. **50**, 63 (1997).
- ¹⁵ W. Schülke, G. Stutz, F. Wohlert and A. Kaprolat, Phys. Rev. B **54**, 14381 (1996).
- ¹⁶ E. E. Lafon and C. C. Lin, Phys. Rev. **152**, 579 (1966).
- ¹⁷ B. I. Lundqvist and C. Lydén, Phys. Rev. B **4**, 3360 (1971).

- ¹⁸ P. Eisenberger, L. Lam, P.M. Platzman and P. Schmidt, Phys. Rev. B **6**, 3671 (1972).
- ¹⁹ S. Wakoh and J. Yamashita, J. Phys. Soc. Jpn. **35**, 1402 (1973).
- ²⁰ W. Y. Ching and J. Callaway, Phys. Rev. B. **9**, 5115 (1974).
- ²¹ Y. Kubo, J. Phys. Soc. Jpn. **65**, 16 (1996).
- ²² Y. Kubo, J. Phys. Soc. Jpn. **66**, 2236 (1997).
- ²³ D. Singh, *Planewaves, pseudopotentials and the LAPW method*, (Kluwer Academic, Boston, 1994).
- ²⁴ L. Lam and P. Platzman, Phys. Rev. B **9**, 5122 (1974).
- ²⁵ D. A. Cardwell and M. J. Cooper, J. Phys. : Cond. Matt. **1**, 9357 (1989).
- ²⁶ P. Blaha, K. Schwarz and J. Luitz, **WIEN97**, Vienna University of Technology 1997. (Improved and updated Unix version of the original copyrighted WIEN-code, which was published by P. Blaha, K. Schwarz, P. Sorantin and S. B. Trickey, in Comp. Phys. Comm. **59**, 399 1990).
- ²⁷ J. P. Perdew, S. Burke and M. Ernzerhof, Phys. Rev. Lett. **77**, 3865 (1996).
- ²⁸ D. R. Lide (ed.), *CRC Handbook of Chemistry and Physics*, 74th edition, (CRC Press, London, 1994).
- ²⁹ V. L. Moruzzi, A. R. Williams and J. F. Janak, *Calculated electronic Properties of Metals*, (Pergamon, New York, 1978).
- ³⁰ G. Lehman and M. Taut, Phys. Status Solidi **54**, 469 (1974).
- ³¹ U. von Barth and L. Hedin, J. Phys. B **16**, 3687 (1983).
- ³² L. Lam and P. Platzman, Phys. Rev. B **9**, 5128 (1974).
- ³³ Our work on ferromagnetic Ni, which will be published elsewhere, demonstrates that in Ni, the non local corrections affect the EMD. This is in agreement with the results in ref.¹⁴.
- ³⁴ G. E. W. Bauer and J. R. Schneider, Phys. Rev. B **31**, 681 (1985).
- ³⁵ S. M. Kim and A. T. Stewart, Phys. Rev. B **11**, 2490 (1975).
- ³⁶ J. Meingailis and S. Debeneditti, Phys. Rev. **145**, 400 (1966).
- ³⁷ S. S. Rajput, R. Prasad, R. M. Singru, W. Triftshauser, A. Eckert, G. Kögel, S. Kaprzyk and A. Bansil, J. Phys. : Cond. Matt. **5**, 6419 (1993).
- ³⁸ L. Oberli, A. A. Manuel, R. Sachot, P. Descouts, M. Peter, L. P. L. M. Rabou, P. E. Mijnders, T. Hyodo and A. T.

Stewart, Phys. Rev. B **31**, 1147 (1985).

³⁹ J. J. Donaghy and A. T. Stewart, Phys. Rev. **164**, 391 (1967).

Table I

Directions	Fermi surface radii	
	FP-LAPW	Experimental
k_{100}	0.578	0.577 ± 0.004
k_{110}	0.611	0.604 ± 0.004
k_{111}	0.585	0.586 ± 0.004

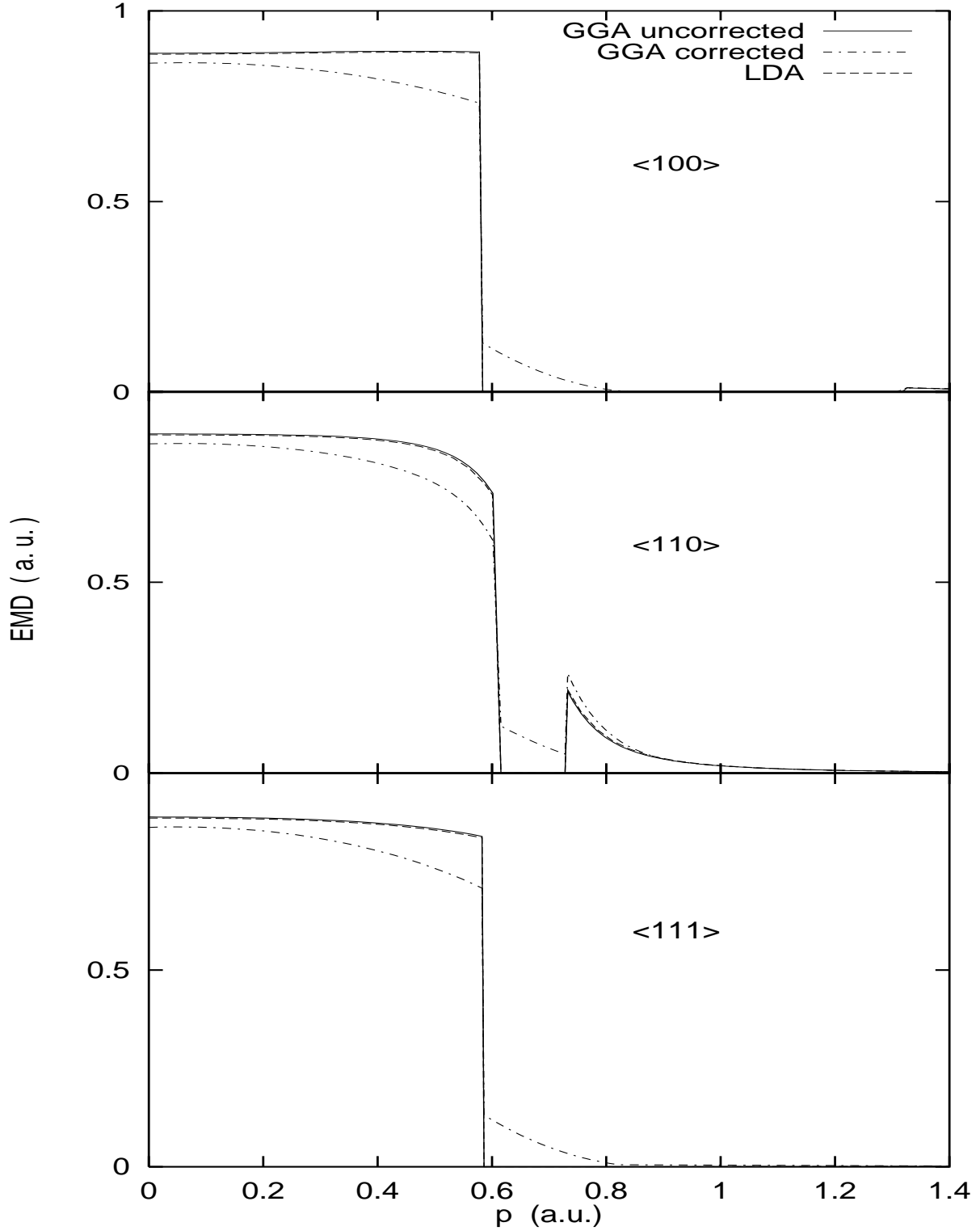


FIG. 1. Electron momentum densities along $\langle 100 \rangle$, $\langle 110 \rangle$ and $\langle 111 \rangle$ directions.

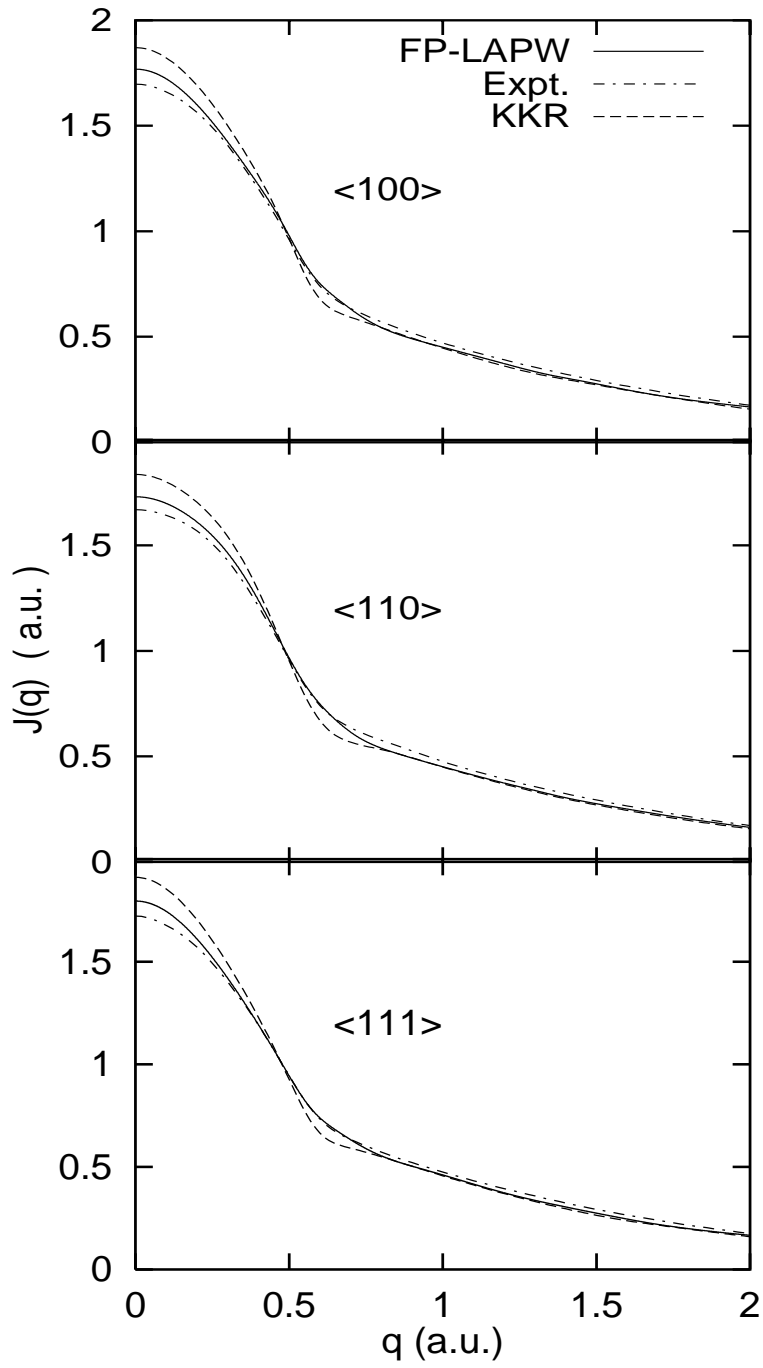


FIG. 2. Compton profiles along $\langle 100 \rangle$, $\langle 110 \rangle$ and $\langle 111 \rangle$ directions.

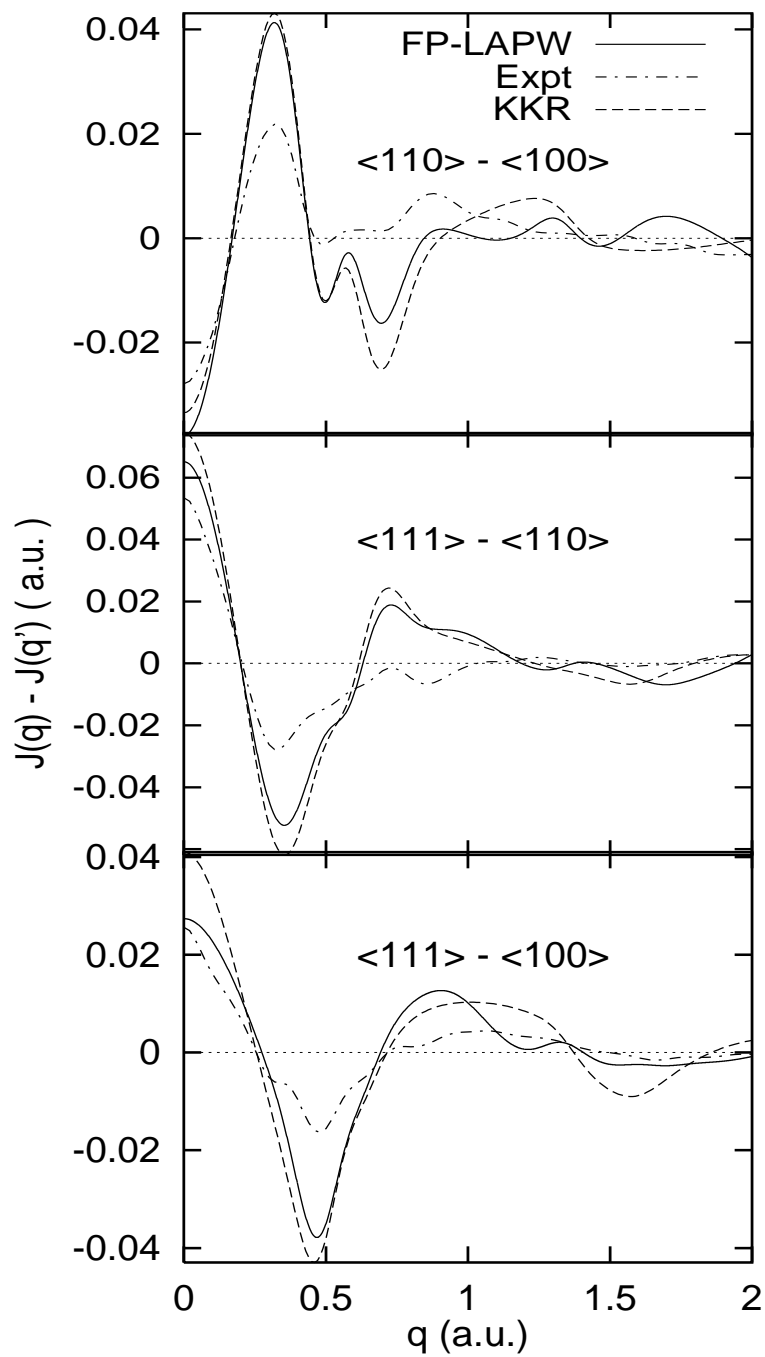


FIG. 3. Anisotropies of the Compton profiles between various directions.

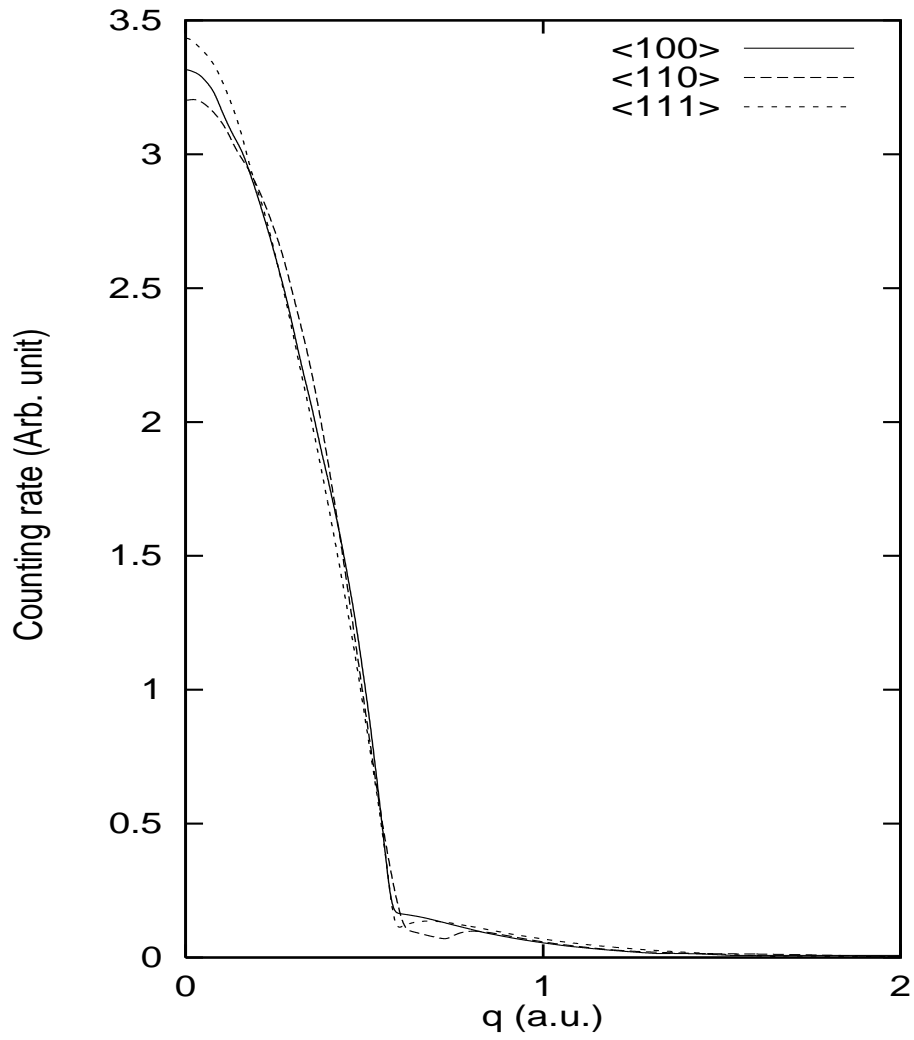


FIG. 4. One-dimensional ACPAR curves along $\langle 100 \rangle$, $\langle 110 \rangle$ and $\langle 111 \rangle$ directions

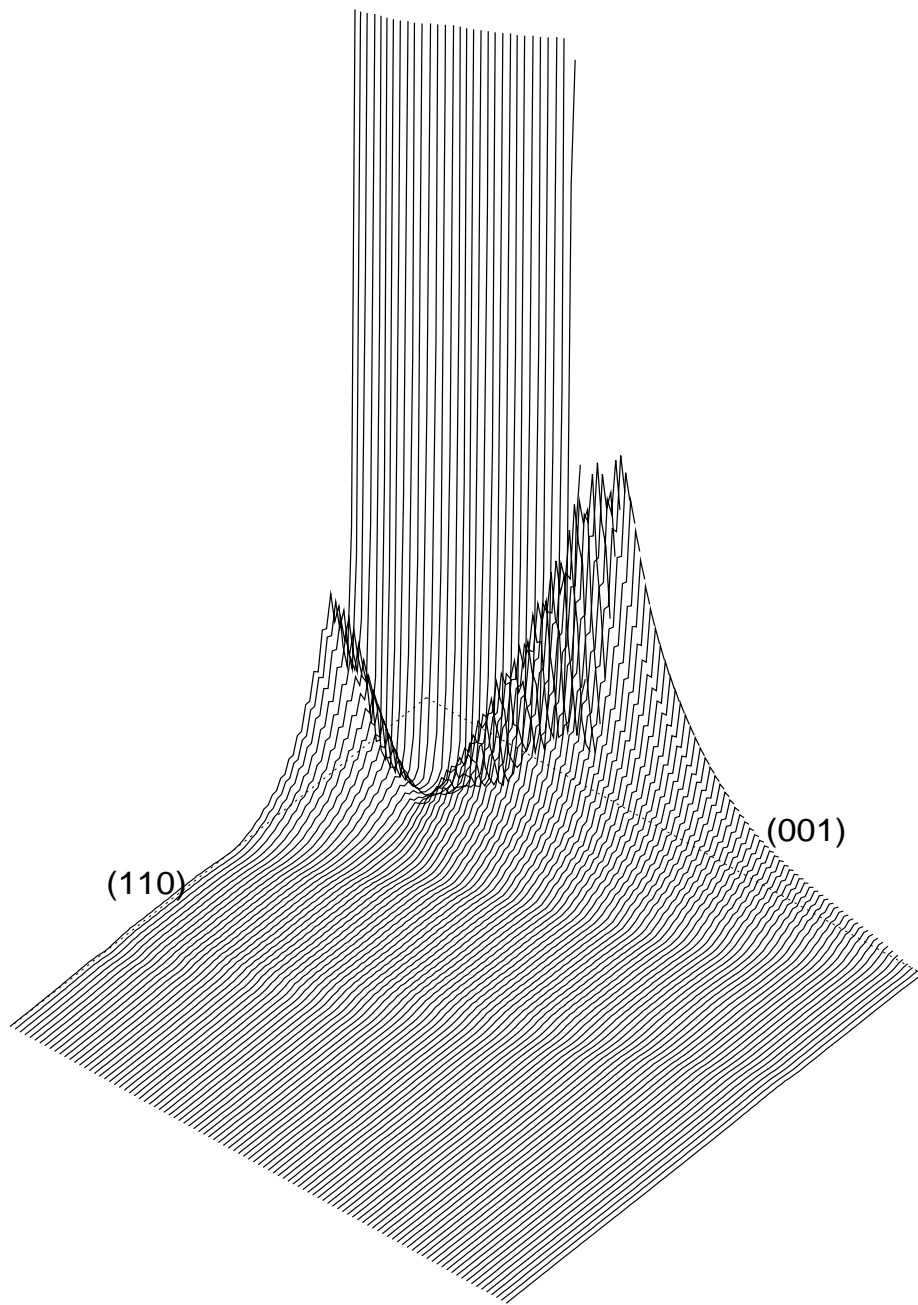


FIG. 5. Two-dimensional ACPAR plot of Li in the $(1\bar{1}0)$ plane.

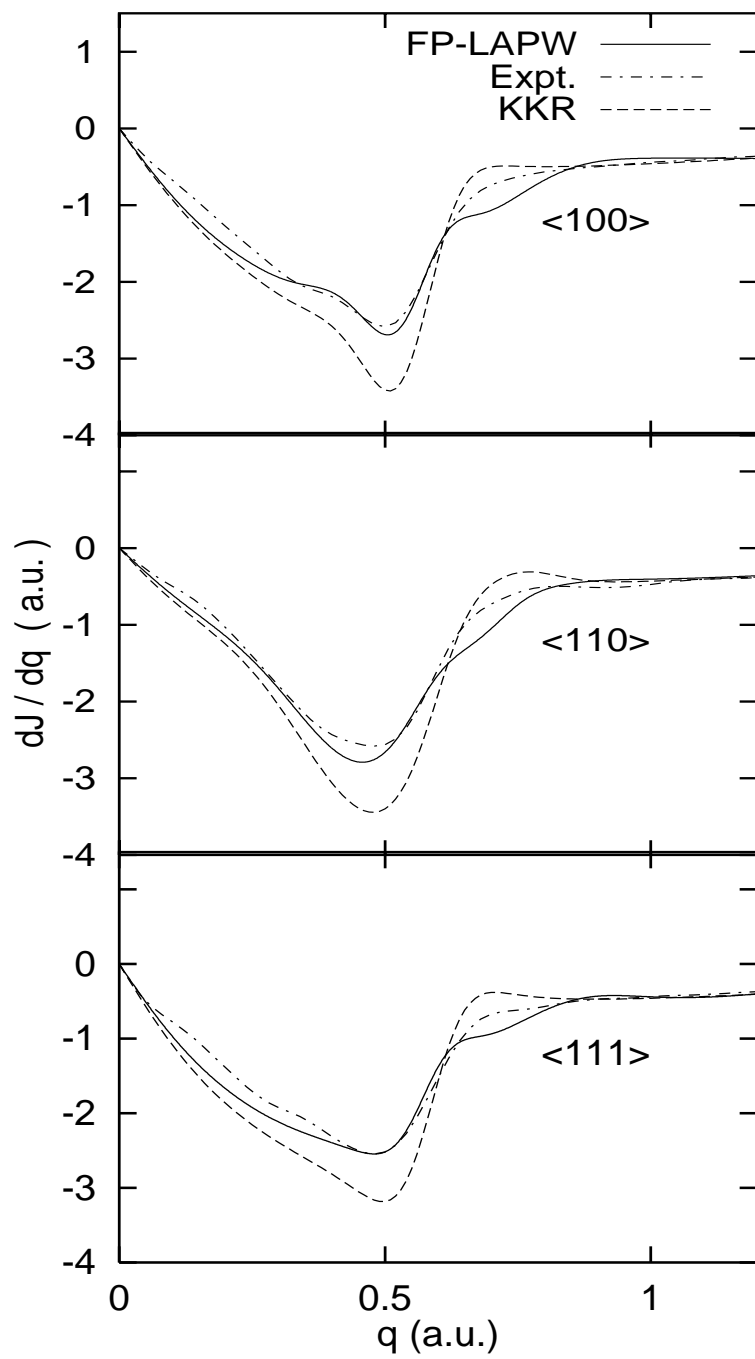


FIG. 6. Derivative of the Compton profiles along $\langle 100 \rangle$, $\langle 110 \rangle$ and $\langle 111 \rangle$ directions.

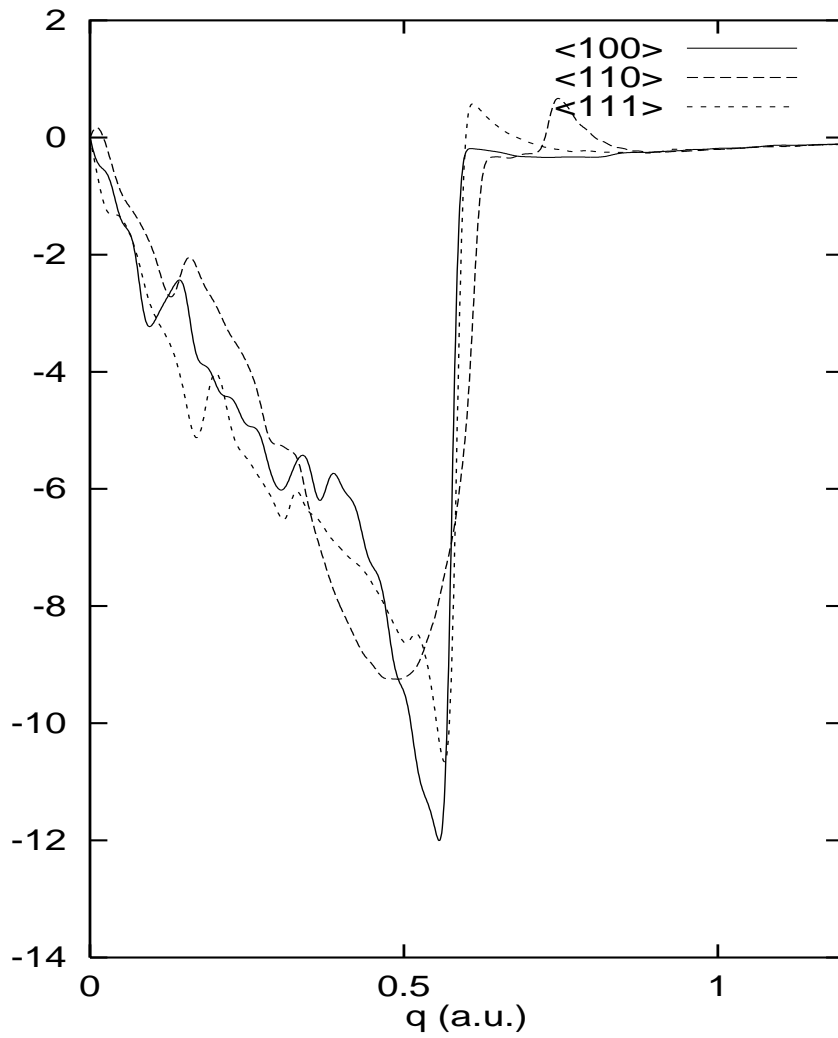


FIG. 7. Derivative of one-dimensional ACPAR curves along $\langle 100 \rangle$, $\langle 110 \rangle$ and $\langle 111 \rangle$ directions